PHYSICAL REVIEW E **77**, 046118 (2008)

Mapping giant magnetic fields around dense solid plasmas by high-resolution magneto-optical microscopy

Jaivardhan Sinha, Shyam Mohan, and S. S. Banerjee*
Department of Physics, Indian Institute of Technology, Kanpur-208016, U. P., India

Subhendu Kahaly and G. Ravindra Kumar†
Tata Institute of Fundamental Research, 1 Homi Bhabha Road, Mumbai 400 005, India

(Received 14 April 2007; published 29 April 2008)

We investigate the distribution of magnetic fields around dense solid plasmas generated by intense *p*-polarized laser ($\sim 10^{16}$ W cm^{-2}, 100 fs) irradiation of magnetic tapes, using high sensitivity magneto-optical microscopy. By investigating the effect of irradiation on the magnetic tape, we present evidence for axial magnetic fields and map out the spatial distribution of these fields around the laser generated plasma. By using the axial magnetic field distribution as a diagnostic tool we uncover evidence for angular momentum associated with the plasma.

DOI: 10.1103/PhysRevE.77.046118 PACS number(s): 52.38.Fz, 52.70.Ds, 52.70.Kz, 75.60.Ch

I. INTRODUCTION

Contemporary fascination with ultralarge, megagauss (MG) scale magnetic fields is inspired by (a) their unique influence on fundamental properties of condensed matter systems at low temperatures at one end and (b) their role in hot, dense, highly ionized complex plasmas that mimic astrophysical scenarios at the other. Fields as large as 700 MG—the largest on earth—found in intense picosecond laser produced solid plasmas [1], offer tantalizing possibilities to simulate the behavior of neutron stars in the laboratory [2]. At low temperatures, giant magnetic fields might enable the exploration of exotic quantum fluctuation driven phase transitions [3,4] and new phenomena such as the now well known fractional quantum Hall effect [4] associated with two-dimensional electron gas in semiconductors. Pulsed, giant magnetic fields also impact current efforts to realize "fast ignition" of laser fusion [5] as they crucially modify relativistic electron transport, a key physics issue of this scheme. Recently it has been shown that ultrashort laser pulse irradiation on magnetic materials can be used for investigating ultrafast spin dynamics [6,7]. We have recently demonstrated azimuthal megagauss field pulses of subpicosecond duration generated during intense laser pulse irradiation and extracted the hitherto intractable electrical conductivity of the plasma from them [8]. Knowledge of the spatial and temporal behavior of large magnetic fields associated with laser plasmas is crucial for applying them in fundamental study as well as manipulation of electronic properties of materials.

II. RESONANCE ABSORPTION AND AZIMUTHAL MAGNETIC FIELDS IN LASER INDUCED PLASMAS

Strong azimuthal magnetic fields [$\sim O(100)$ MG] are generated in dense plasmas using the explosive ionization of a solid target by intense, ultrashort laser pulses [1], which generate mega amperes of relativistic "hot" electron currents directed into the target. Magneto-optical (MO) techniques (Faraday and Cotton Mouton) have been used for probing the *azimuthal* magnetic field created by resonance absorption (RA) in plasmas [8]. Briefly, during RA an inhomogeneous, dense plasma interacts with a *p*-polarized laser pulse incident at an oblique angle to the target normal exciting plasma waves [9]. Damping of this plasma wave generates a jet of hot electrons, directed along the target normal, which in turn gives rise to azimuthal fields [8] parallel to the surface of the target. An issue of fundamental significance is whether fields with other symmetries (e.g., axial) are also present under RA conditions. To date, axial magnetic fields in intense laser produced plasmas have been demonstrated only in experiments using normally incident circularly polarized laser light [10]. In this paper we not only present clear evidence for *axial* magnetic fields generated by *p-polarized* light excitation (i.e., under RA conditions) but also obtain unique information about the distribution of these axial fields around the irradiated spot. We employ the high sensitivity magneto-optical microscopy (MOM) technique, which has been used extensively in recent studies of condensed matter systems [11,12]. Faraday rotation, which is *blind* to the azimuthal magnetic field, enables reliable quantitative imaging of the axial magnetic field distribution via MOM. In our experiment, the axial field distribution generated around the laser plasma is imprinted on a magnetic recordable media (magnetic tape) after the tape is irradiated with 100 femtosecond *p*-polarized laser pulses at intensities in the range of 10^{15}–10^{16} W cm^{-2}. Dramatic changes in the magnetic domain patterns are observed on the tape after laser irradiation. By analyzing the distribution of axial magnetic fields recorded on the magnetic tape with MOM, we infer the presence of azimuthal circulating currents in the plasma thereby indicating broken rotational symmetry.

III. EXPERIMENTS

We irradiated the magnetic tape (T) mounted in a vacuum chamber with *p*-polarized pulses from a tabletop terawatt

*satyajit@iitk.ac.in
†grk@tifr.res.in

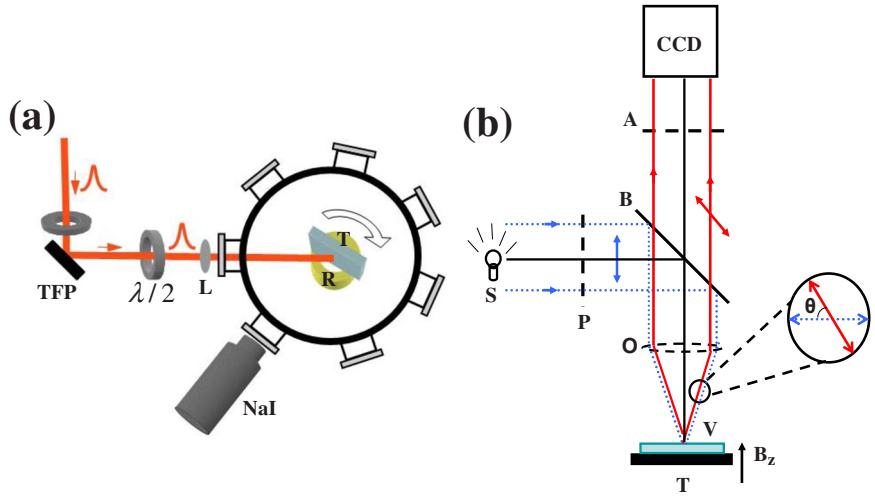

FIG. 1. (Color online) (a) Schematic of the irradiation setup: TFP—thin film polarizer, λ/2—half wave plate, *L*—lens, *R*—rotation stage, *T*—target (magnetic tape), and NaI—scintillation detector. (b) Schematic of MOM setup consisting of light source (*s*), linear polarizer (*P*), beam splitter (*B*), objective (*O*), MOM indicator film (*V*), tape (*T*), and analyzer (*A*). Also indicated is the local magnetic field direction (B_z). The blowup shows the state of linear polarization in the incident (blue, dotted line) and reflected beam (red, solid line).

laser (806 nm, 10 Hz, and 100 fs) [8] at a 45° angle of incidence. Figure 1(a) is the sketch of the experimental setup used for irradiation. Each laser shot is focused by lens (*L*) on a fresh spot on the tape. The intensity is controlled using a half wave plate (λ/2) before a thin film polarizer (TFP) (λ/2). Another λ/2 ensures that *p*-polarized light irradiates target (*T*). A time-gated NaI(Tl) scintillating detector is used to record the hard x-ray bremsstrahlung spectrum. The Doppler shift of the reflected laser pulse is measured by an optical spectrometer (blue shift, given by the expanding plasma, which is useful for inferring the plasma expansion velocity). The magnetic tape used as the target consists of nanometer sized γ-Fe_2O_3 particles suspended in a polymeric, nonmagnetic matrix [13,14]. While the magnetic properties of the nanometer sized ferromagnetic particles are of current interest [15], we will be concerned only with the bulk magnetic response of the ferromagnetic tapes, as the MOM imaging technique measures the magnetization response averaged over a large number of nanoparticles. The typical size of the tapes used was 7×4 mm^2 and thickness $O(100$ nm) [13,14]. Energy dispersive x-ray spectroscopic (EDAX) analysis in a scanning electron microscope (model QUANTA-200, from FEI) indicated a layer of Fe_2O_3 constituting the tape and the magnetic properties of the tape were investigated using a commercial vibrating sample magnetometer (VSM) (model EV7-VSM; ADE Technologies), with a sensitivity of 10^{-5} emu. After laser irradiation, the tapes were transferred from the irradiation chamber to the MOM setup. Faraday rotation [16] is the basis of the MOM setup, which has a reflecting type polarizing microscope (Carl Zeiss, model: Axio Tech Vario) and a Peltier cooled charge coupled device (CCD) camera (Andor, iXon, 512 $\times$512 pixels, 16 bit, 85% quantum efficiency at 550 nm). The ray diagram in our MOM setup is shown in Fig. 1(b). During the experiment, a material with high Verdet's constant (v) [ferrite garnet films (FGF), which are bismuth substituted yttrium iron garnet film deposited on gadolinium gallium garnet substrate, marked *V* in Fig. 1(b)] is placed in direct contact with the irradiated tape [*T*, in Fig. 1(b)]. The linearly polarized incident light [dotted ray in Fig. 1(b)] undergoes Faraday rotation upon reflection from *V*. The angle of Faraday rotation $\theta=B_z v(2d)$, where d is the thickness of the FGF film and B_z is the local field perpendicular to the tape surface (axial) placed underneath the FGF film. A high sensitivity CCD camera is placed after the analyzer (which is adjusted nearly perpendicular to the linear polarizer). The CCD captures the Faraday rotated light intensity variations which correspond to the spatial distribution of the axial magnetic field, viz., $B_z(x,y)$. The local intensity of the image (i.e., the gray level) is directly related to the value of $B_z(x,y)$ and its direction. In this mode of operation the magnetic field sensitivity is 0.5 G (though much higher sensitivity is possible [12]) with an optical spatial resolution (of the microscope) =0.5 μm.

As is well known [13,14,16], information in a magnetic recordable tape is encoded via a unique arrangement of magnetic domains on the tape. Figure 2(a) is a schematic of a cross section of the magnetic tape, which shows a typical arrangement of magnetic domains with in-plane magnetization (shown by horizontal arrows). The circular arrows drawn outside the tape represent the dipolar magnetic field distributed around the domain edges. The thick vertical white and black lines in the schematic correspond to the z component (perpendicular to the tape surface) of the magnetic field (B_z) pointing either out of ($+B_z$) or into the tape surface ($-B_z$), at the magnetic domain edges. Using MOM we can identify the magnetic domain edges on the tape from the contrast difference of the Faraday rotated light intensity due to $+B_z$ and $-B_z$ at the magnetic domain edges. Figure 2(b) shows the MOM image of magnetic domains in a region of the tape where data are encoded. In the MOM image, a single strip of magnetic domain is characterized by bright and dark lines with gray in between [see the area inside the dotted lines in the inset of Fig. 2(b)]. The white and black lines are magnetic domain edges corresponding to $+B_z$ pointing out of and $-B_z$ pointing into the tape surface, respec-

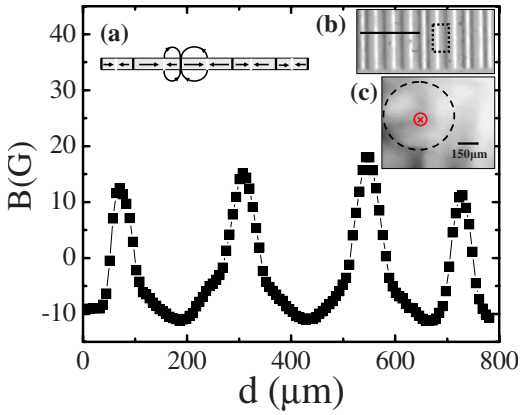

FIG. 2. (Color online) $B_z(x)$ across a region of a prerecorded magnetic tape. (a) Schematic for orientation of magnetization in the magnetic tape. (b) MOM image of a prerecorded magnetic tape. (c) Effect of terawatt laser pulse irradiation on a prerecorded magnetic tape (refer to the text for details). The symbol ⊗ represents the location of the center of the laser pulse irradiation.

tively. The setup is calibrated by measuring θ for known magnetic field values. Using this calibration scheme the $B_z(x,y)$ across the tape surface can be inferred. In Fig. 2 the main panel shows the $B_z(x)$ profile measured across the solid horizontal black line on the tape in Fig. 2(b). In Fig. 2(c), we show an MOM image in a prerecorded region of the tape irradiated with femtosecond laser pulse with peak intensity of 10^{16} W cm^{-2}. The region around the laser irradiation spot is encircled. It is interesting to note that sharp lines observed with MOM on the prerecorded tape before irradiation, cf. Fig. 2(b), have completely faded away after the irradiation, cf. Fig. 2(c). It is plausible that magnetic fields generated due to the laser pulse irradiation cause a scrambling of the magnetic domains on the tape. In the subsequent sections we will investigate the fields generated around the laser pulse irradiation.

IV. MOM IMAGING OF FIELDS RECORDED ON AN UNMAGNETIZED TAPE DURING LASER PULSE IRRADIATION

To determine the pristine nature of the magnetic fields generated due to intense *p*-polarized laser pulse irradiation, a region of the tape *devoid of predefined magnetic domains* was chosen for irradiation, viz., we irradiated an unrecorded tape without magnetic domains like those shown in Fig. 2(b). The tape was irradiated at six locations (arranged on the vertices of a hexagon) with single shots from the femtosecond laser pulse with energy 6.0–6.4 mJ. The spot size of the irradiating laser pulse was 20 μm. The heating generated by the laser irradiation is highly local as the medium of the tape is a nonconducting polymer, which aids in the creation of the plasma at the irradiation site. Figure 3(a) shows the MOM image of the six irradiated spots. Figure 3(b) shows the line scan ($B_z(x)$) across the dark line in Fig. 3(a). It is seen that $B_z(x)$ changes sign across the irradiated spot, viz., the field varies from +70 G on the periphery of the spot to −70 G in the center of the spot. We will discuss the significance of the

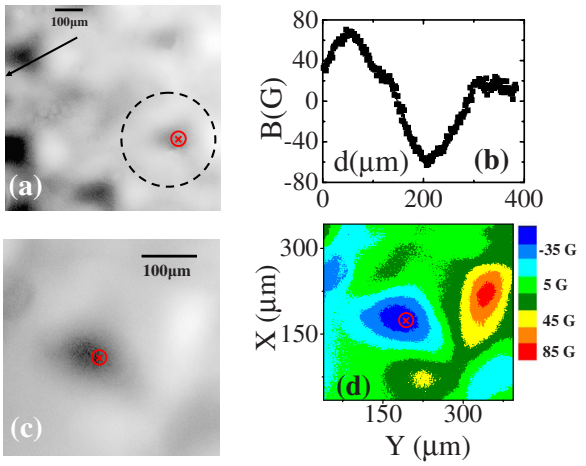

FIG. 3. (Color online) (a) MOM image of six locations on the irradiated tape. (b) Behavior of B_z [across the solid line in Fig. 3(a)]. (c) Magnified MOM image of a single irradiated spot [refer to the dotted black circled region in Fig. 3(a)]. (d) Contour map of $B_z(x,y)$ around the spot shown in (c). The symbol ⊗ represents the location of the center of the laser pulse irradiation.

sign change of B_z subsequently. The axial magnetic field distribution shows smooth and continuous behavior. In Fig. 3(b) we find that $B_z(x)$ reaches a maximum of +70 G on one edge of the irradiated spot and in a diametrically opposite region on the periphery it is only +20 G, indicating a nonuniform local field profile ($B_z(x,y)$) around the spot. In Fig. 3(c) we show a high magnification MOM image of a single irradiated spot [region within the dashed, black circle in Fig. 3(a)]. Figure 3(d) is the contour plot of the magnetic field distribution ($B_z(x,y)$) deduced from the MO image in Fig. 3(c), where each shade of gray (or color) represents uniform $B_z(x,y)$ values. From Fig. 3(d) it is clear that the axial magnetic field (B_z) generated by the laser pulse irradiation has a complex and highly nonuniform spatial distribution around the irradiated spot. The above features are common to all the six irradiated spots. The essential feature of this complex distribution of axial magnetic fields is that regions with $-B_z$ [pointing into the tape, the black shade on the color bar corresponds to −70 G (bluish regions in color online)] is surrounded with $+B_z$ regions [pointing out of the tape, the gray shade on the color bar corresponds to 5 G (the greenish shade in color online)]. It must be noted that these *axial* magnetic fields stored on the tape are mere remnants of the magnetic field generated during the laser pulse irradiation. Magnetic domains respond to a variable magnetic field on time scales of nanosecond to subnanosecond range [7]. Thus the intense laser induced field which magnetized the tape must have persisted well beyond the duration of the femtosecond laser pulse. The only source of such fields are the magnetic fields frozen around the hot expanding laser generated plasma (that survive for time periods longer than picosecond duration), which magnetizes the tape. From the MOM measurements of Fig. 3, we find that the tape around the laser irradiation spot has acquired a magnetization of few tens of gauss. At first glance from above one could argue that the tape was subjected to a magnetic field of a few tens of gauss after laser pulse irradiation. However, such an infer-

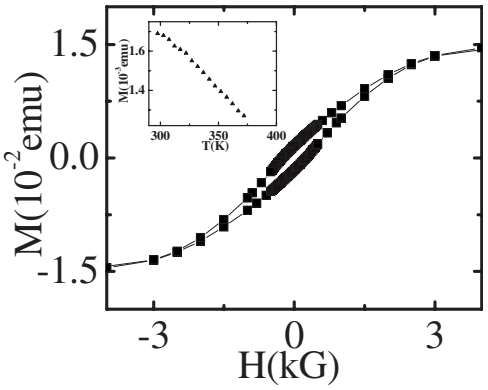

FIG. 4. $M-H$ hysteresis loop of the tape. The inset is the behavior of the remnant magnetization of the tape as a function temperature (refer to the text for details).

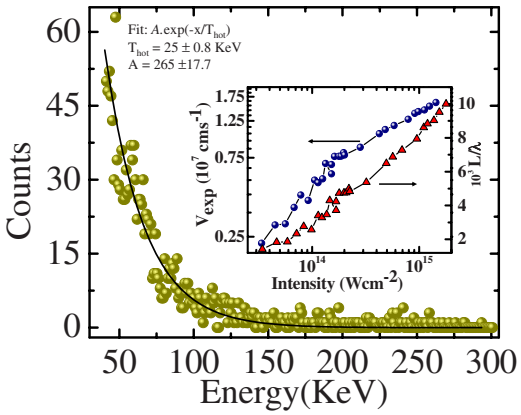

FIG. 5. (Color online) Bremsstrahlung x-ray emission from the laser produced plasma on the irradiated spot. The solid line is a fit through data. The inset shows a variation of plasma expansion velocity (blue circles) and scale length (red triangles) with intensity (refer to the text for details).

ence is inconsistent with the fact that the tape is subjected to a heat pulse during laser irradiation, and hence magnetization of the order of a few tens of gauss stored in the tape would decay down to subgauss levels due to heating. It can be concluded that the tape was subjected to a much larger magnetic field after laser pulse irradiation, which magnetized the tape to larger magnetization values. Heating of the tape in the vicinity of the laser pulse causes decay in the magnetization to the levels measured on the tape in Fig. 3. The demagnetization process of magnetic materials at ultrafast time scales such as the system we are investigating is a rich, complex, and contemporary problem [17]. Due to the strongly nonequilibrium nature of the process we attempt in this paper to make a crude estimate for the extent of momentary heating of the tape based on the amount of demagnetization of the tape. We base our rough estimate of the temperature to which the region around the laser spot is momentarily subjected to, by comparing the magnetization around the laser irradiated region measured via MOM with bulk magnetization measurements of the tape.

V. MOMENTARY HEATING OF THE TAPE DUE TO LASER PULSE IRRADIATION

Shown in Fig. 4 is the ferromagnetic hystersis loop of the magnetic tape recorded on a VSM. The magnetization response of the tape *saturates* beyond 0.3 T of applied magnetic field. The saturation magnetization of the tape is estimated to be $O(1\ \mathrm{T})$, which is close to the remnant magnetization measured for this tape. The intense laser irradiation heats up the tape to a temperature which is estimated here. Using the VSM we measure the temperature (T) dependence of the remnant magnetization (M_{rem}) of the tape. To measure M_{rem}, a magnetic field of 1 T, which saturates the magnetization of the tape, is applied and subsequently switched off. The inset of Fig. 4 shows the variation of magnetization with temperature. A temperature dependence of the type $M_{\mathrm{rem}}(T)=M_{\mathrm{rem}}(T=0)+T(dM_{\mathrm{rem}}/dT)$, with $M_{\mathrm{rem}}(T=0)=1.5$ T and $dM_{\mathrm{rem}}/dT=-26.4$ G/°K, is found. Hence, to reach $M_{\mathrm{rem}}\sim 100$ G (measured through $B_z(x,y)$ $(=4\pi M_{\mathrm{rem}}$ at $H=0)$ using MOM [cf. Fig. 3(b)], the magnetic particles in the tape in the vicinity of the laser irradiation spot may have been exposed to $T\geq O(600\ \mathrm{K})$. This observation concurs well with simulations predicting temperatures of $O(10^3\ \mathrm{K})$ in a localized region [18] around the laser irradiation site. Due to localized heating effects a large magnetization stored in the tape would decay down to a few 100 gauss. Thus, temperature and relaxation effects obscure the observation of the peak value of the magnetic field recorded on the magnetic tape during the intense laser pulse irradiation. It needs to be emphasized here that while local heating of the polymeric tape decreases the M_{rem} value, it cannot reproduce the change in sign of $B_z(x,y)$ as seen in the line scan Fig. 3(b) or the field distribution shown in Fig. 3(d).

VI. PARAMETERS OF THE LASER GENERATED PLASMA

The intense laser irradiation pulse creates a hot dense plasma above the tape surface. We present some basic characteristics of this plasma. The hot electrons created by the resonance absorption (RA) process cause the emission of hard x-ray bremsstrahlung, shown in Fig. 5. The temperature of the hot electrons can be estimated from the exponential behavior of the bremsstrahlung spectrum from the plasma (cf. Fig. 5) recorded in our setup with time-gated NaI(Tl) scintillating detectors [19]. A plasma temperature of 25 keV (T_{hot} in Fig. 5) is obtained which is consistent with earlier reports [20]. This temperature also scales correctly with the cold (bulk) plasma temperature of 100 eV, estimated at the laser intensity used in this paper [19,21]. The inset of Fig. 5 presents the plasma expansion velocity deduced from reflectivity measurements and corroborated by Doppler shift data. As we can see, the highest expansion velocity of 1.5×10^7 cm/s gives a plasma length of 0.01 laser wavelengths at the end of the laser pulse. This indicates that the plasma is essentially flat during the laser pulse irradiation. The plasma density is assumed to vary exponentially with distance toward the vacuum. The superhot dense plasma cools as it expands from a size of 0.01 laser wavelengths at the end of

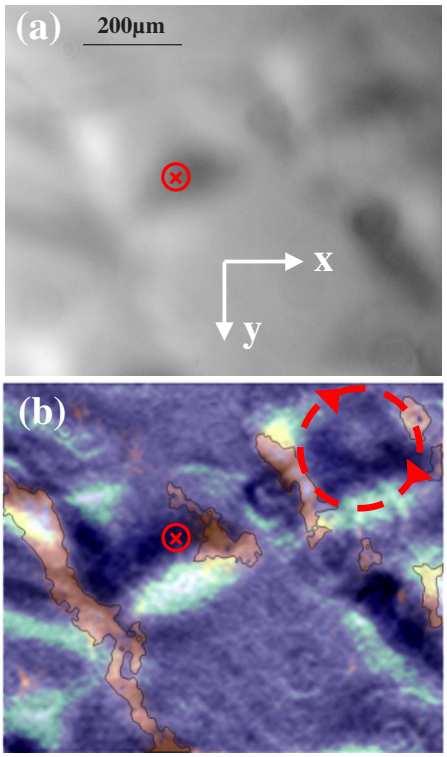

FIG. 6. (Color online) (a) MOM image of irradiated regions on the tape. (b) Derivative of the MO image shown in (a) (cf. text). The red dashed circle schematically represents circulation of azimuthal currents responsible for the axial fields. The symbol ⊗ represents the location of the center of the laser pulse irradiation.

laser pulse irradiation. Instabilities in this hot expanding plasma generate the axial magnetic fields around it whose distribution we investigate subsequently.

VII. DETERMINING THE CURL OF THE AXIAL MAGNETIC FIELD DISTRIBUTION STORED ON THE TAPE

By determining the curl of $B_z(x,y)$ [where $\vec{B}=B_z(x,y)\hat{k}$], we uncover a symmetry in the complex distribution of axial fields noted in Fig. 3(d). From an MOM image of an irradiated spot as in Fig. 6(a), we determine $B_z(x,y=\text{const})$ and $B_z(x=\text{const},y)$ and take their derivatives in the x and y directions, to obtain the curl of the axial magnetic fields around an irradiated region in Fig. 6(b). In Fig. 6(b) the bright region (light blue) corresponds to maximum values of $\vec{\nabla}\times\vec{B} \approx \hat{i}(\partial B_z/\partial y)$ (where $\hat{i}(\partial B_z/\partial y) \gg \hat{j}(\partial B_z/\partial x)$ along the x direction) and the contoured gray region (orange) corresponds to maximum values for $\vec{\nabla}\times\vec{B}\approx\hat{j}(\partial B_z/\partial x)$ (where $\hat{j}(\partial B_z/\partial x) \gg \hat{i}(\partial B_z/\partial y)$ along the y direction). The nonzero nature of the curl of $\vec{B}_z(x,y)$ implies a circulation ($\vec{\nabla}\times\vec{B}\propto\vec{J}$, where $\vec{J}$ is the current density; displacement current ~ 0 in a plasma). In Fig. 6(b) the dashed (red) circle is a schematic of the vector field and represents circulation. We believe our observation of a nonzero circulation associated with $B_z(x,y)$ with its axis perpendicular to the tape surface is due to the

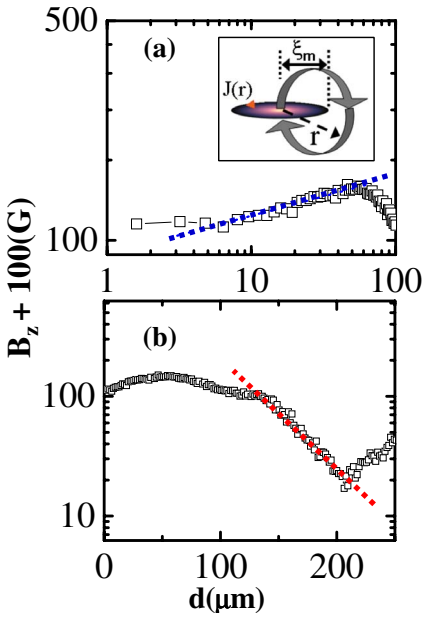

FIG. 7. (Color online) (a) $\log(B_z+100\ \text{G})$ vs $\log(d)$ variation far away from the laser irradiated spot. The inset shows the schematic of a 2D current sheet, $J(r)$ (a model for a horizontal cross section of plasma vortex). (b) $\log(B_z+100\ \text{G})$ vs d variation close to irradiation spot.

circulation of charges in the momentarily generated plasma above the tape. The finite angular momentum generated in the plasma is associated with a magnetic dipole moment. Information about the perpendicular components of the dipolar magnetic field distributed around the hot expanding plasma gets "fossilized" or stored in the remnant magnetization of the tape.

VIII. MODEL

The circulation of charges in the plasma is akin to vortex motion observed during turbulent flow of rotating fluids. To understand the spatial dependence of the dipolar magnetic field distribution [cf. Figure 3(b)], we approximate the vortex motion in the plasma as an ideal 2D circular sheet of current. A well known feature pertaining to vortices in fluids is that the circulation (vorticity) decays away from the vortex core and the decay are especially strong for low viscosity fluids [22]. A schematic representation of a horizontal cross section through the plasma is shown in Fig. 7(a). Shown as the shaded disk is the 2D current sheet circulating in the plasma vortex, whose strengths decay rapidly away from the plasma core [represented as bright near the center and darker around the edges of the disk in the schematic of Fig. 7(a)]. The current density in the sheet is modeled as $J(r) = J_0 \exp[-(r-\xi_0)/\xi_m]$ and $J=0$ for $r<\xi_0$, where r is the radial coordinate within the plasma, ξ_0 is the minimum radius of the current sheet (= radius of the laser spot ~ 10 μm), and ξ_m is the radius of the rotating plasma, ~ 100 μm. As shown in the inset of Fig. 7(a), ξ_m is the length scale over which the *dipolar* magnetic field distributed (shown as circulating gray arrows) around the hot expanding plasma

changes direction [$\xi_m \sim 100$ μm, is deduced from the sign change in $B_z(x)$ in Fig. 3(b)]. For distance $r > \xi_m$, using an Amperian loop shown as the gray circulating arrow in the inset of Fig. 7(a), the axial component of the *dipolar* magnetic field on the $z=0$ plane is $B_z(r \to \infty) \sim \mu_0 \xi_m J_0 \exp(\xi_0/\xi_m)/2\pi r$. From above we approximate that for $r \gg \xi_m$, $B_z(r) \propto r^n$, where n is negative. In Figs. 7(a) and 7(b), for the sake of representing the data of Fig. 3(b) on log scale, 100 G has been added to the data in Fig. 3(b). Clearly the linear variation in the log-log plot [see the dotted line in Fig. 7(a)], confirms the above approximate r^n variation expected for the *dipolar* field around the plasma. At $r < \xi_m$, using Biot-Savart's law we get $B_z(r \to 0) \sim (\mu_0 \xi_m J_0 / 2r) \exp[-(r-\xi_0)/\xi_m][\exp(r/\xi_m)-1]$. For $r \ll \xi_m$, using $[\exp(r/\xi_m)-1] \approx r/\xi_m$, we find $|\ln B_z(r)| \propto r$, which is confirmed via a linear variation (dotted line) observed in the semilogarithmic plot in Fig. 7(b). Using our previously estimated lower bound axial field of 0.3 T at $r=200$ μm and with the $B_z(r \to \infty)$ expression, we evaluate $\mu_0 \xi_m J_0 \exp(\xi_0/\xi_m) \sim 3 \times 10^{-4}$ T$-m$. Using this we get $B_z(r \to 0) \sim (3 \times 10^{-4}/2\xi_m) \sim 1.5$ T. The estimated value depends on our approximation of the size of the hot expanding plasma, $\xi_m \sim 100$ μm, which is an overestimation.

We confirm our estimate of B_z frozen around the laser generated plasma in a separate measurement using an electromagnet for applying an external magnetic field perpendicular to a prerecorded magnetic tape. We observe that fields of at least 0.3 T had to be applied before the unirradiated prerecorded tapes with domains similar to Fig. 2(b) showed the effect of fading of domains, similar to that produced as a result of laser pulse irradiation [cf. Fig. 2(c)]. We therefore infer that fading of prerecorded domains as in Fig. 2(c) is due to the generation of large axial magnetic fields overwhelming the domain patterns on the tape and orienting all the domains in the same directions. The domains are found to be affected at distances as large as 200 μm from the irradiated spot, from which we conclude that at distances as large as 20 times the radius of the irradiating laser beam (10 μm) magnetic fields of at least 0.3 T are created (note that saturation magnetization of the tape limits this estimate). We point out that this estimate of the field at the center of the irradiated spot is very conservative; generated fields could be much larger than this.

A dramatic manifestation of the effect of the burst of a large axial magnetic field generated during the intense laser pulse irradiation is shown in Fig. 8. By comparing magnetic domain patterns shown in Fig. 2(b) to those in Fig. 8, we find a complete change in their shapes. Figure 8 shows that in a region of the tape close to the laser pulse irradiation the sequential pattern of magnetic domains has completely disappeared. In the lower portion of the image (across the dashed line) in Fig. 8 we find that the lines more or less appear in the bright-dark-bright sequence similar to Fig. 2(b), although they are fainter than that in the unirradiated tape [viz., Fig. 2(b)]. However, in the upper portion of the image in Fig. 8, viz., across the black line, we find that the bright and dark lines have completely disappeared from the central region of the image.

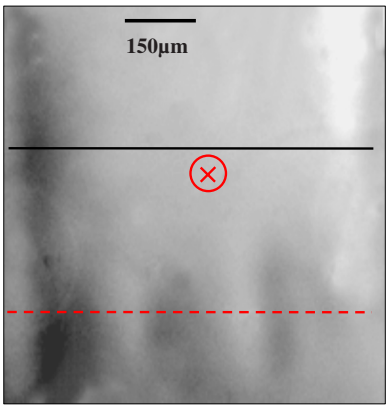

FIG. 8. (Color online) Effect of terawatt laser pulse irradiation on the magnetic domains in regions of a prerecorded magnetic tape (refer to the text for details). The symbol ⊗ represents the location of the center of the laser pulse irradiation.

IX. CONCLUSION

In conclusion, we have presented clear evidence for giant axial magnetic fields under resonance absorption of intense, pulsed laser light in solid dense plasmas. We present the high resolution (micron scale) spatial maps of these giant fields using high sensitivity MOM. Our study reveals broken continuous rotational symmetry in the plasma due to the presence of angular momentum associated with a vortex of circulating charges in the plasma. We have analyzed our results with a model for the plasma vortex. We believe that our work would stimulate future theoretical attempts to understand the instabilities in the plasma which generates the vortex and subsequently, large axial magnetic fields. It is possible that the well known massive azimuthal fields in some way couple to the plasma to generate the angular momentum in the plasmas associated with intense laser matter interactions. It may also prove interesting and rewarding to draw analogies of the plasma circulation described here with other well known vortex phenomena. Based on our observation of the ability of the intense *p*-polarized laser pulse to scramble magnetic information, we speculate on the potential of combining magneto-optical imaging with intense *p*-polarized femtosecond laser pulses for possible applications with respect to ultrafast encoding of information and reading the information on magnetic media.

ACKNOWLEDGMENTS

S.S.B. would like to acknowledge the support from Professor A. K. Grover and Professor Eli Zeldov. S.S.B. also acknowledges the funding received from Director, IIT Kanpur, CSIR, India, Grant No. 03(1066)/06/EMR-II and DST, India Grant No. SR/S2/CMP-17/2005. G.R.K. thanks DAE-SRC, India for an Outstanding Investigator grant.

[1] M. Tatarakis *et al.*, Nature (London) **415**, 280 (2002).
[2] D. Lai, Rev. Mod. Phys. **73**, 629 (2001).
[3] S. Sachdev, Science **288**, 475 (2000).
[4] R. R. Du, A. S. Yeh, H. L. Stormer, D. C. Tsui, L. N. Pfeiffer, and K. W. West, Phys. Rev. Lett. **75**, 3926 (1995), and references therein.
[5] R. Kodama *et al.*, Nature (London) **412**, 798 (2001).
[6] F. Hansteen, A. Kimel, A. Kirilyuk, and T. Rasing, Phys. Rev. Lett. **95**, 047402 (2005).
[7] C. D. Stanciu, F. Hansteen, A. V. Kimel, A. Tsukamoto, A. Itoh, A. Kirilyuk, and T. Rasing, Phys. Rev. Lett. **98**, 207401 (2007); Q. Zhang, A. V. Nurmikko, A. Anguelouch, G. Xiao, and A. Gupta, Phys. Rev. Lett. **89**, 177402 (2002); S. B. Choe *et al.*, Science **304**, 420 (2004); W. K. Hiebert *et al.*, J. Appl. Phys. **92**, 392 (2002).
[8] J. A. Stamper, Laser Part. Beams **9**, 841 (1991); Y. Sakagami *et al.*, Phys. Rev. Lett. **42**, 839 (1979); Y. Sakagami, H. Kawakami, and C. Yamanaka, Phys. Rev. A **21**, 882 (1980); A. S. Sandhu, A. K. Dharmadhikari, P. P. Rajeev, G. R. Kumar, S. Sengupta, A. Das, and P. K. Kaw, Phys. Rev. Lett. **89**, 225002 (2002); A. S. Sandhu, G. R. Kumar, S. Sengupta, A. Das, and P. K. Kaw, Phys. Rev. E **73**, 036409 (2006).
[9] W. L. Kruer, *The Physics of Laser Plasma Interactions* (Addison-Wesley, Reading, MA, 1988); A. S. Sandhu *et al.*, Phys. Rev. Lett. **95**, 025005 (2005).
[10] Y. Horovitz, S. Eliezer, A. Ludmirsky, Z. Henis, E. Moshe, R. Shpitalnik, and B. Arad, Phys. Rev. Lett. **78**, 1707 (1997).
[11] U. Welp, V. K. Vlasko-Vlasov, X. Liu, J. K. Furdyna, and T. Wojtowicz, Phys. Rev. Lett. **90**, 167206 (2003).
[12] A. Soibel *et al.*, Nature (London) **406**, 282 (2000); S. S. Banerjee *et al.*, Phys. Rev. Lett. **93**, 097002 (2004) and references therein.
[13] C. D. Mee, *The Physics of Magnetic Recording* (North-Holland Publishing Company, Amsterdam, 1964), Vol. 2, pp. 176–235.
[14] R. J. Veitch, A. Ilmer, and W. Lenz, IEEE Trans. Magn. **35**, 2787 (1999).
[15] E. Tronc *et al.*, J. Magn. Magn. Mater. **221**, 63 (2000).
[16] A. A. Polyanskii, D. M. Feldmann, and D. C. Larbalestier, in *Magneto-Optical Characterization Techniques*, edited by D. A. Cardwell and D. S. Ginley, Handbook of Superconducting Materials (Institute of Physics Publishing UK, Bristol, UK, 2003), Vol. 2, pp. 1551–1567.
[17] R. Knorren, K. H. Bennemann, R. Burgermeister, and M. Aeschlimann, Phys. Rev. B **61**, 9427 (2000); G. P. Zhang and W. Hübner, Phys. Rev. Lett. **85**, 3025 (2000).
[18] T. E. Glover, J. Opt. Soc. Am. B **20**, 125 (2003).
[19] P. P. Rajeev and G. R. Kumar, Opt. Commun. **222**, 9 (2003).
[20] M. Anand *et al.*, Appl. Phys. Lett. **88**, 181111 (2006).
[21] P. P. Rajeev, S. Banerjee, A. S. Sandhu, R. C. Issac, L. C. Tribedi, and G. R. Kumar, Phys. Rev. A **65**, 052903 (2002).
[22] Milne—L. M. Thomson, *Theoretical Hydrodynamics*, 5th ed. (Dover Publications, Inc., New York, 1996).